A High-Field EPR Study of $P_{700}^{+\bullet}$ in Wild-Type and Mutant Photosystem I from *Chlamydomonas reinhardtii*[†,‡]

Alexander Petrenko,[§] Anna Lisa Maniero,[∥] Johan van Tol,[⊥] Fraser MacMillan,[@] Yajing Li,[§] Louis-Claude Brunel,[⊥] and Kevin Redding*[,§]

Departments of Chemistry and Biological Sciences, University of Alabama, Tuscaloosa, Alabama 35487-0336, Department of Physical Chemistry, University of Padova, via Loredan, 2, Padova 35131, Italy, Center for Interdisciplinary Magnetic Resonance, National High Magnetic Field Laboratory, Florida State University, 1800 East Paul Dirac Drive, Tallahassee, Florida 32310, and Institute for Physical and Theoretical Chemistry, J. W. Goethe University, Marie Curie Strasse 11, D-60439 Frankfurt am Main, Germany

Received August 15, 2003; Revised Manuscript Received December 23, 2003

ABSTRACT: High-frequency, high-field EPR at 330 GHz was used to study the photo-oxidized primary donor of photosystem I ($P_{700}^{+\bullet}$) in wild-type and mutant forms of photosystem I in the green alga *Chlamydomonas reinhardtii*. The main focus was the substitution of the axial ligand of the chlorophyll *a* and chlorophyll *a*′ molecules that form the P_{700} heterodimer. Specifically, we examined PsaA-H676Q, in which the histidine axial ligand of the A-side chlorophyll *a*′ (P_A) is replaced with glutamine, and PsaB-H656Q, with a similar replacement of the axial ligand of the B-side chlorophyll *a* (P_B), as well as the double mutant (PsaA-H676Q/PsaB-H656Q), in which both axial ligands were replaced. We also examined the PsaA-T739A mutant, which replaces a threonine residue hydrogen-bonded to the 13^1-keto group of P_A with an alanine residue. The principal **g**-tensor components of the $P_{700}^{+\bullet}$ radical determined in these mutants and in wild-type photosystem I were compared with each other, with the monomeric chlorophyll cation radical ($Chl_z^{+\bullet}$) in photosystem II, and with recent theoretical calculations for different model structures of the chlorophyll a^+ cation radical. In mutants with a modified P_B axial ligand, the g_{zz} component of $P_{700}^{+\bullet}$ was shifted down by up to 2×10^{-4}, while mutations near P_A had no significant effect. We discuss the shift of the g_{zz} component in terms of a model with a highly asymmetric distribution of unpaired electron spin in the $P_{700}^{+\bullet}$ radical cation, mostly localized on P_B, and a deviation of the P_B chlorophyll structure from planarity due to the axial ligand.

The initial electron donor in photosystem I (PS1)[1] is P_{700}*, the excited state of a pair of excitonically coupled chlorophyll (Chl) molecules (Chl *a*′ and Chl *a*; see Figure 1), which are coordinated by subunits PsaA and PsaB, respectively (*1*, *2*). The first stage of electron transfer forms the cation radical $P_{700}^{+\bullet}$. The electronic properties of $P_{700}^{+\bullet}$ are determined by the nature of electronic states of the oxidized Chl dimer, as well as its interaction with the protein environment. Surprisingly, the 2.5-Å resolution crystal structure of PS1 from *Thermosynechococcus elongatus* (*1*) revealed that P_{700} is not a Chl *a* dimer, as had been assumed, but a heterodimer of Chl *a* (P_B) and Chl *a*′ (P_A), the 13^2-epimer of Chl *a* (see Figure 1). The side chain of a threonine residue (PsaA-Thr739) is in position to donate a hydrogen bond to the 13^1-keto oxygen. (The numbering system refers to the polypeptides of *Chlamydomonas reinhardtii*.) The hydroxyl group of this Thr residue also seems to participate in a hydrogen bonding network involving a bound water molecule, which donates a H-bond to the 13^2-methyl ester oxygen of P_A. This water has three other potential hydrogen bond partners around it: hydroxyls of PsaA-Ser607 and PsaA-Tyr603 and the backbone oxygen of PsaA-Gly739. However, P_B has no comparable H-bond network. Thus, P_{700} is fundamentally asymmetric, and the H-bond to the 13^1-keto oxygen would seem to be the most important functional feature of this asymmetry, since this keto group is part of the conjugated π system. These structural features would seem to be consistent with electron nuclear double resonance (ENDOR) measurements of $P_{700}^{+\bullet}$ that estimated a $\geq$5:1 localization of unpaired electron spin on P_B (*3*). However, Fourier transform infrared (FTIR) difference spectra of P_{700} have been interpreted in terms of a model in which the positive charge is shared equally between the two Chls (*4*) (see ref *5* for an alternate interpretation).

[†] This work was supported by a grant from the Department of Energy to K.R. (DE-FG02-00ER15097). F.M. was supported by an EU Marie-Curie Fellowship (ERBCHRXCT940524) and the DFG (SFB472).

[‡] Protein Data Bank entries 1PSS (RC of *Rhodobacter sphaeroides*), 1JB0 (PS1 of *Thermosynechococcus elongatus*), and 1PPR (peridinin−chlorophyll protein of *Amphidinum carterae*) were used.

* To whom correspondence should be addressed: Departments of Chemistry and Biological Sciences, University of Alabama, Tuscaloosa, AL 35487-0336. Phone: (205) 348-8430. Fax: (205) 348-9104. E-mail: Kevin.Redding@ua.edu.

[§] University of Alabama.

[∥] University of Padova.

[⊥] Florida State University.

[@] J. W. Goethe University.

[1] Abbreviations: BChl, bacteriochlorophyll; Chl, chlorophyll; ENDOR, electron nuclear double resonance; EPR, electron paramagnetic resonance; FTIR, Fourier transform infrared; hfc, hyperfine coupling; HF-EPR, high-field (frequency) EPR; P_A, chlorophyll *a*′ on the A-side of P_{700}; P_B, chlorophyll *a* on the B-side of P_{700}; PS1, photosystem I; PS2, photosystem II; RC, reaction center; WT, wild type.

10.1021/bi035466j CCC: $27.50
Published on Web 01/29/2004

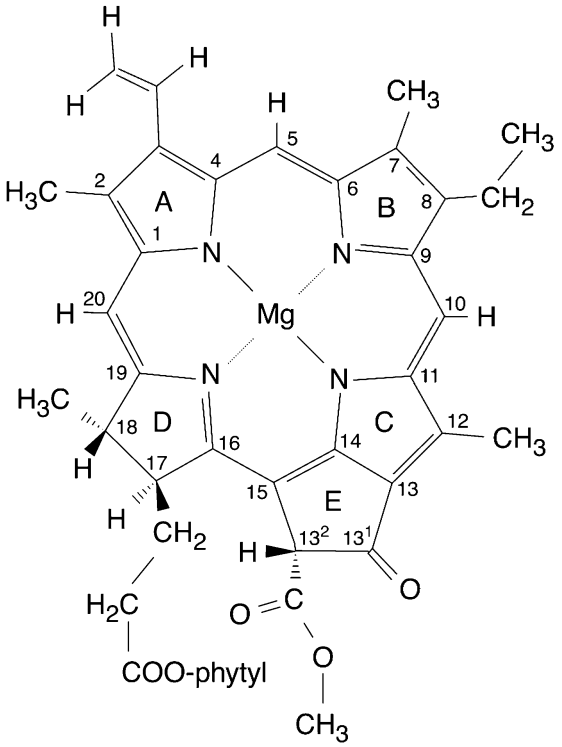

FIGURE 1: Structure and IUPAC numbering system for Chl *a*. The Chl *a*′ isomer has the opposite stereochemistry at position 13^2.

The other major interaction between the P_{700} Chls and their environment is that of the axial ligand and the central Mg(II), which is provided by the protein in the form of two histidine residues: PsaA-His676 (P_A) and PsaB-His656 (P_B). It was previously shown that mutation of the axial ligands could perturb P_{700} (*6*−*8*). While mutation of PsaB-His656 caused shifts of proton hyperfine couplings (hfcs) to the $P_{700}^{+\bullet}$ radical cation, as seen by ENDOR spectroscopy, mutation of the ligand to P_A had almost no effect upon the ENDOR spectrum (*6*, *8*). Thus, it was concluded that the hole was primarily localized on P_B. Interestingly, mutation of PsaA-His676 to Gln did have a noticeable effect upon the P_{700}^+/P_{700} FTIR difference spectrum in the region assigned to the 13^1-keto group (*7*, *9*). Mutations of axial ligands on either side had significant effects upon the P_{700}^+/P_{700} visible difference spectrum and increased the midpoint potential of $P_{700}^{+\bullet}/P_{700}$ (*7*, *8*).

The use of high-frequency, high-field EPR enables the complete resolution of the **g**-tensor of slightly anisotropic radicals, such as organic cofactors. Prisner *et al*. (*10*) were the first to completely resolve the **g**-tensor of $P_{700}^{+\bullet}$, using deuterated PS1 from *T. elongatus* and a frequency of 140 GHz. Use of a sufficiently high field and/or frequency allows resolution of the **g**-tensor without having to resort to deuteration of the sample, which eliminates the large proton hyperfine couplings that would otherwise broaden the EPR lines. Bratt *et al*. (*11*) reported the complete resolution of the $P_{700}^{+\bullet}$ EPR spectrum at 330 GHz using protonated PS1 from spinach. They found essentially identical **g**-tensor principal components as in the previous study, but also found a temperature dependence for g_{xx}, indicating that the $P_{700}^{+\bullet}$ radical may become more anisotropic at lower temperatures. In this study, we have used high-field EPR to resolve completely the **g**-tensor components of $P_{700}^{+\bullet}$ in wild-type PS1 and four mutants in which amino acids serving as axial ligands or H-bond donors have been targeted.

EXPERIMENTAL PROCEDURES

The axial ligand mutants (*7*) and the PsaA-T739A mutant (*5*) have been described. Isolation of thylakoid membranes from *C. reinhardtii* was performed as described previously (*7*). To generate the $P_{700}^{+\bullet}$ radical, concentrated thylakoid membranes were mixed with a small amount of ferricyanide in a Teflon cup and illuminated with strong white light for 10 s before being placed in liquid nitrogen under continuous illumination. The $Chl_Z^{+\bullet}$ sample has been described previously (*12*) and was remeasured at the same time as the $P_{700}^{+\bullet}$ samples.

The HF-EPR spectrometer, as well as a procedure for simulation spectra, has been described previously (*13*). Spectra were recorded at a magnetic field of 11.6−11.7 T and a temperature of 10 K. We used a P-doped Si standard ([P] $\sim 10^{15}$ spins/cm^3) for field calibration and measurement of sample **g**-tensor principal values. Spectra of $P_{700}^{+\bullet}$ were recorded before and after addition of the *g* standard; the standard was added through the waveguide tube so that the sample would not be moved. The P-Si standard *g* value was calibrated using Mn(II) in MgO at 240 GHz. We have used the effective *g* value of Mn^{2+} in MgO standard [g_{eff} = 2.00101 ± 0.00005 (*14*)] and obtained the *g* value of our reference P-Si standard ($g_r = 1.99854 \pm 0.00005$), which is in good agreement with the literature value of 1.99850 ± 0.00010 (*15*). The simulations were fits to the data made via a home-written program that allows for an admixture of dispersion and absorption, and optimization of the *g* values and line widths. All fits were done using a Gaussian line shape only. In some spectra, we observed lines from Mn(II) contaminating the samples. When possible, these were simulated as well (not shown).

RESULTS AND DISCUSSION

Figure 2 shows the high-field EPR spectra recorded for *C. reinhardtii* $P_{700}^{+\bullet}$ cation radicals from the wild type (WT), from single mutants PsaA-T739A, PsaA-H676Q, and PsaB-H656Q, and from double mutant PsaA-H676Q/PsaB-H656Q. All spectra were simulated, and the simulation parameters are given in Table 1.

When the *g* values for the wild-type and mutant PS1s were compared, a relationship was clearly seen between the side of the P_{700} dimer perturbed by the mutation and the g_{zz} component. Only mutation of the axial ligand to P_B (PsaB-H656Q and PsaA-H676Q/PsaB-H656Q mutants) caused a significant shift in the g_{zz} value. The slight differences between the g_{zz} value in the P_A mutants (PsaA-H676Q and PsaA-T739A) and in WT were within the limits of experimental error.

Results of previous ENDOR studies supported the model in which the unpaired electron spin distribution within the $P_{700}^{+\bullet}$ radical cation is strongly localized to P_B (see ref *16* for a recent review). The structural inequivalence of P_A and P_B is determined first by the difference in their configurations, with P_A being the 13^2-epimer of Chl *a*. Second, P_A accepts hydrogen bonds from side chains of PsaA-ThrA739 and PsaA-Tyr731 and from a water molecule, while there are no hydrogen bonds to P_B. The electronic states of $P_{700}^{+\bullet}$

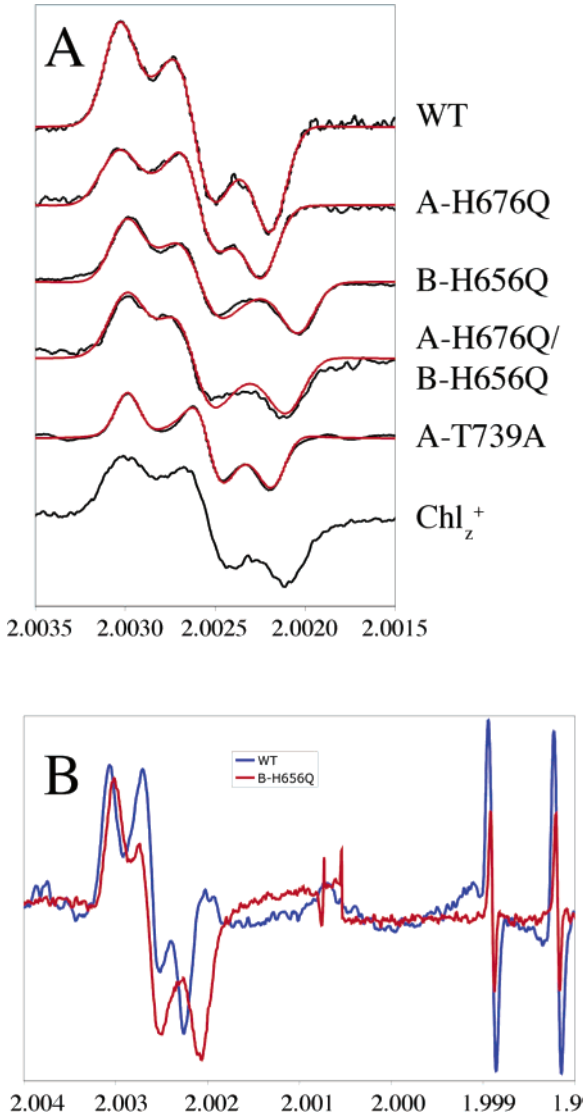

FIGURE 2: High-field EPR spectra of $P_{700}^{+\bullet}$ in *C. reinhardtii* PS1. Spectra were recorded at 10 K and a magnetic field strength of approximately 11.6−11.7 T, using frequencies of 324−327 GHz. The magnetic fields were calibrated using a P/Si standard (see Experimental Procedures). Spectra were scaled and offset to enable easy comparison in panel A. Spectra are shown in black, with simulations in red. In panel B is a comparison of the spectra from WT (blue) and the PsaB-H656Q mutant (red), including the signal from the P/Si standard (at $g = 1.998-1.999$), to enable direct comparison.

are also perturbed by interaction of the Chls with their axial ligands, and the perturbations may not be equal across the two sides. These structural and environmental differences are thought to influence the spin density distribution in $P_{700}^{+\bullet}$ such that most of it is localized on one of the P_{700} Chls, consistent with the results of hyperfine spectroscopy (*3*, *17*−*19*). The fact that mutation of the P_B axial ligand affected the $P_{700}^{+\bullet}$ ^{1}H ENDOR spectrum (primarily by increasing the hfc assigned to the 12-methyl protons), while mutation of the P_A axial ligand had no effect, was used to identify P_B as the chlorophyll on which the spin was localized in $P_{700}^{+\bullet}$ (*6*, *8*). However, one might well ask what the assignment would have been had mutants in the H-bond donor (PsaA-Thr739) been the first ones analyzed, as mutation of this residue caused a *decrease* in the same hfc (*20*, *21*). It is not straightforward to rationalize the effect of a mutation on one side of P_{700} (13^1-keto group of P_A) upon the hfc from a group on the other side (12-methyl group of P_B). Although a decrease in the hfc from the 12-methyl protons of P_B is expected if spin density is redistributed from P_B to P_A after removal of the H-bond to P_A, one might also expect a decrease in all the hfcs assigned to P_B and a corresponding increase in the hfcs assigned to P_A; these were not observed (*20*, *21*). While one might argue that "indirect effects" could explain this, such an argument would undermine the claim that ENDOR spectroscopy is the "method of choice" for obtaining information about spin localization. By its nature, hyperfine spectroscopy will be sensitive to differences in local spin density; however, the **g**-tensor is more of a global measure of spin distribution within the system, and high-field EPR is therefore a complementary method for examining environmental effects upon a radical. On the basis of our analysis of mutations in the axial ligands to P_A and P_B and in the H-bond donor to the 13^1-keto of P_A, we also conclude that the spin is strongly localized on P_B, consistent with the previous conclusions from hyperfine measurements.

Mutation of the P_B axial ligand provoked a decrease in g_{zz}, while mutation of the axial ligand or H-bond donor to P_A had no large effect. While we can explain the *specificity* of the effect by localization of the spin on P_B, the effect itself (shift of g_{zz}) requires some discussion. Previously, changes in g_{xx} caused by mutation of H-bond donors have been observed and theoretically explained (see ref *22* for a recent example). To the best of our knowledge, this is the first time that a shift in g_{zz} of a cofactor radical caused by a mutation in a nearby residue has been observed, and it was not expected. We now turn to a discussion of this effect and its possible origins.

It is known from density functional theory (DFT) quantum chemical calculations that the optimized structure of Chl *a* is very planar *in vacuo* (*23*, *24*). However, this planarity is seriously perturbed in P_B (*2*, *25*) due, at least in part, to its interaction with the histidine axial ligand. In P_B, the position of the central Mg(II) deviates from the mean plane of the four nitrogen atoms by 0.4 Å (see Figure 3A). There is also a significant deviation of atoms 13^1 and 13^2 of ring V from the macrocycle mean plane. Moreover, the peripheral vinyl group at position 3 (see Figure 1) is also rotated ~90° out of plane so that the plane of the vinyl group is almost perpendicular to the main plane of the macrocycle. This same dihedral angle characterizes the position of the acetyl group in the P_L bacteriochlorophyll found in the X-ray structure of the P_{865} special pair in reaction centers from *Rhodobacter sphaeroides* [PDB entry 1PSS (*26*)]. This out-of-plane position of the 3-vinyl group of P_B might explain the tilt between the *z*-axis of the P_{700}^+ **g**-tensor and the molecular *z*-axis of P_B (*27*). The study of the spin-correlated $P_{700}^{+\bullet}A_1^{-\bullet}$ radical pair by Zech *et al.* (*27*) preceded publication of the high-resolution PS1 structure (*1*); they expected that the 3-vinyl group would be in plane, since it could not participate in hydrogen bonding, unlike the 3-acetyl group of BChl. A similar explanation was put forward (*28*) for the tilt between the *z*-axis of the **g**-tensor of P_{865}^+ and the molecular *z*-axes of the BChls (*29*).

The perturbation of the planarity of the electronic π-system could explain changes in g_{zz}. In the PsaB-H656Q mutant (and PsaA-H676Q/PsaB-H656Q), we might expect a return of P_B toward a more planar structure after mutation of the axial

Table 1: Experimental **g**-Tensor Components of Primary Donor Cation Radical $P_{700}^{+\bullet}$ in Wild-Type and Mutant Photosystem I of *C. reinhardtii* and Theoretical **g**-Tensor Components for Model Chl $a^{+\bullet}$ Structures

	g_{xx}[a]	g_{yy}[a]	g_{zz}[a]	$g_{xx} - g_{zz}$[b]	$g_{xx} - g_{yy}$[b]	$g_{yy} - g_{zz}$[b]
WT	2.00304	2.00262	2.00220	84.7	41.6	43.1
PsaA-H676Q	2.00305	2.00260	2.00224	80.4	45.1	35.3
PsaB-H656Q	2.00301	2.00260	2.00205	96.2	40.8	55.4
PsaA-H676Q/PsaB-H656Q	2.00300	2.00261	2.00210	89.8	38.3	51.5
PsaA-T739A	2.00301	2.00255	2.00220	80.3	45.9	34.4
$Chl_Z^{+\bullet}$ (PS2)[c]	2.00304	2.00252	2.00213	91	52	39
(Chl $a^{+\bullet}$) model[d]	2.00291	2.00258	2.00197	94	33	61
(Chl $a^{+\bullet}$) model[e]	2.00290	2.00278	2.00219	71	12	59

[a] Experimental error of $3-4 \times 10^{-5}$. [b] The difference ($g_{ii} - g_{jj}$) is multiplied by a factor of 10^5. [c] From ref *12*. [d] This represents a structure of chlorophyll optimized *in vacuo* (*13*). [e] This represents a structure of antenna chlorophyll in *A. carterae* (*13*).

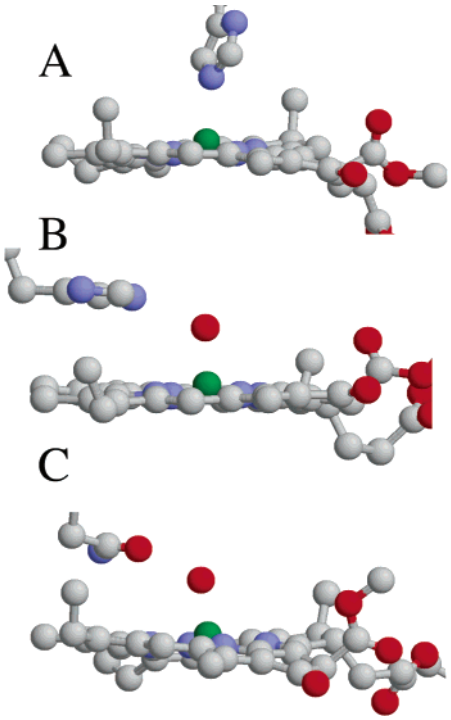

FIGURE 3: Structures of various chlorophylls with distorted planarity. In each case, the chlorophyll is show from the side as a ball-and-stick model using CPK colors (central Mg in green). (A) P_B of *T. elongatus* PS1 (molecule 1012 of PDB entry 1JB0), including the axial ligand, PsaB-His660 (homologous with His656 of *C. reinhardtii*). (B) Antenna chlorophyll in the peridinin−chlorophyll protein of *A. carterae* (molecule 601 of PDB entry 1PPR), including the water molecule serving as the axial ligand, coordinated by His66. (C) Chlorophyll $ec2_A$ of *T. elongatus* PS1 (molecule 1021 of PDB entry 1JB0), including the water molecule serving as the axial ligand, coordinated by PsaB-Asn591.

ligand histidine. Therefore, in accordance with the argument described above and assuming that in $P_{700}^{+\bullet}$ the unpaired electron is mostly on P_B, g_{zz} of $P_{700}^{+\bullet}$ in WT should be different from g_{zz} of $P_{700}^{+\bullet}$ in mutants of the axial ligand of P_B.

The deviation of Chl $a^{+\bullet}$ from planarity would shift g_{zz} from the value in planar Chl $a^{+\bullet}$. There is a question of which kind of deviation would contribute most heavily to the shift of g_{zz}: the deviation of Mg(II) from the macrocycle plane or the vinyl group rotation. There was a difference of 22×10^{-5} in the values of g_{zz} calculated by RHF-INDO (*13*), based on either the optimized *in vacuo* structure of Chl *a* or the chlorophyll in the peridinin−chlorophyll antenna protein from *Amphidinum carterae* (*30*) used as a model for a monomeric Chl species (see Table 1). Examination of the *A. carterae* structure reveals that, unlike the planar *in vacuo* structure, this chlorophyll actually deviates from planarity due to axial ligation by a water molecule of the central Mg(II) such that its position deviates from the mean plane of the four nitrogen atoms by 0.36 Å (Figure 3B), although the 3-vinyl group remains in plane. The same effect of deviation of Mg(II) from the mean plane of chlorophyll and bacteriochlorophyll cation free radical models was shown in a DFT study of axial Mg ligation by water molecules (*31*). Water molecules also serve as axial ligands to the central Mg(II) of both accessory chlorophylls in PS1 (*32*), and they exhibit a similar deviation from planarity (Figure 3C). Because of the similar deviation of Mg(II) observed in both P_B of PS1 and the antenna chlorophyll of *A. carterae*, we might expect a similar value for Δg_{zz} in $P_{700}^{+\bullet}$ of WT PS1, assuming that the unpaired electron in $P_{700}^{+\bullet}$ is mostly localized on one of the Chls. The maximal experimental difference that we observed is $\sim 15 \times 10^{-5}$ (Table 1), which is not far from the theoretical estimation of 22×10^{-5} by RHF-INDO (*13*).

It should be noted that the effect observed here consists of not only a shift of the g_{zz} component but also a conservation of the g_{xx} and g_{yy} values. As we can see from the data in Table 1, the RHF-INDO calculations (*13*) did not predict conservation of the g_{yy} component. One possible reason for that is a difference in vinyl group orientation; it is in plane in the antenna chlorophyll of *A. carterae* and out of plane in P_B of PS1. However, it is also possible that semiempirical calculations (*13*), and the theory (*33*) on which these methods are based, are not always sufficiently reliable. The effects on *g* factor calculations should also be considered at the DFT level of theory (*34*−*37*). Although application of DFT to *g* factor calculations of large systems suffers from quantitative inaccuracy, it can be quite successful in prediction of general trends. In recent *g* factor DFT calculations (*37*) for a model of the BChl cation radical with perturbed planarity of the electronic π-system due to the rotation of the 3-acetyl group, variation of the **g**-tensor anisotropy (as measured by $\Delta g = g_{xx} - g_{zz}$) was observed. Variation of Δg during such rotation was within the limits of $\sim 170 \times 10^{-5}$, with a maximum value at $\sim 30-40°$ out of plane, and shifts in g_{zz} mostly accounted for this variation. It is difficult to make a semiquantitative estimation of that effect in our case based on the results published in ref *37*, because there are many undetermined factors that can influence the result. For example, the data published in ref *37* do not allow one to determine the relative contribution of paramagnetic (spin−orbit/orbital Zeeman) and diamagnetic (relativistic mass correction and gauge correction) terms. In the recent very precise DFT

calculations of the **g**-tensor for quinones (*35*), it was shown that the contribution to the g_{zz} component could range from domination by the spin−orbit coupling term to domination by the diamagnetic term for different quinones and model solvated complexes of quinones. At the same time, at the qualitative level, we might expect a similar effect for the shift of g_{zz} in P_B, as well as conservation of g_{xx} and g_{yy}, due to the rotation of the 3-vinyl group, as was seen for rotation of the 3-acetyl group in $BChl^+$. However, because of the difference in spin−orbit coupling constants between the acetyl oxygen in BChl and the vinyl carbon in Chl *a* (*33*), we might also expect that the magnitude of Δg_{zz} caused by rotation of the corresponding substituent at position 3 would be smaller in Chl than in BChl.

Thus, a model of localization of unpaired electron spin in the $P_{700}^{+\bullet}$ cation radical on P_B, coupled with its nonplanar structure, may reasonably explain the experimentally observed negative shift of g_{zz} seen in the PsaB-H656Q mutant by a return of P_B toward a planar (or near-planar) structure after mutation of the axial ligand histidine. Small changes in the distribution of unpaired electron spin between P_A and P_B, due to changes in the protein environment, might also change the energy difference between the two chlorophylls in $P_{700}^{+\bullet}$, with a resulting influence upon the reduction potential of P_{700}^+/P_{700} (*38*, *39*) and Δg_{zz}, but these are likely less significant. Our conclusions on the differences between the g_{zz} components of $P_{700}^{+\bullet}$ in PsaB-H656Q and PsaA-H676Q/PsaB-H656Q (as well as among WT, PsaA-H676Q, and PsaA-T739A) are limited by the error of measurement of the **g**-tensor principal values with respect to the reference sample ($\pm 3 \times 10^{-5}$). It should also be noted that the quality of the spectrum for the double mutant was lower than the others, due to the ~10-fold reduction in the PS1 content of this mutant (*7*).

In Figure 2, the $P_{700}^{+\bullet}$ EPR spectra are also compared to that of $Chl_Z^{+\bullet}$ from PS2 (*12*, *40*, *41*), which has been used as a representative monomeric chlorophyll cation radical. We note that the g_{zz} value of $Chl_Z^{+\bullet}$ is similar to that of $P_{700}^{+\bullet}$ in the mutants affecting the axial ligand of P_B. However, the relevance of this fact is uncertain, as the current limited resolution of the PS2 structures (*42*, *43*) precludes a similar analysis of this Chl in terms of its planarity or coordination. Similar observations of a difference in the g_{zz} values of $P_{700}^{+\bullet}$ and $Chl_Z^{+\bullet}$ have been made by Poluektov and colleagues (*44*) in their study of the electronic structure of these radicals in deuterated PS1 and PS2 at 130 GHz; they found that the g_{zz} of $P_{700}^{+\bullet}$ was higher than that of $Chl_Z^{+\bullet}$ by 21×10^{-5}. Our data are in agreement with their results, except for a shift in the absolute *g* values, which is due to the use of a different *g* value for Mn(II) in the MnO/MgO standard.

CONCLUSIONS

In this work, we report for the first time the effect of mutations upon the high-field EPR (330 GHz) spectra of the $P_{700}^{+\bullet}$ radical cation. The only mutations to cause significant changes were those that affected the axial ligand of P_B, which allowed an independent identification of P_B as the spin-carrying chlorophyll of $P_{700}^{+\bullet}$, consistent with prior interpretations of hyperfine spectroscopy. Furthermore, contrary to expectations, we have observed shifts in the g_{zz} component caused by mutation of the P_B axial ligand. Comparison of these results with results of theoretical estimations of the *g* factor for different models of the Chl $a^{+\bullet}$ radical cation led us to explain the changes in the g_{zz} component in terms of a deviation of the Chl structure from planarity.

ACKNOWLEDGMENT

We are grateful to Brent Boudreaux and Feifei Gu for preparing some of the thylakoid membranes used in this work.

REFERENCES

1. Jordan, P., Fromme, P., Witt, H. T., Klukas, O., Saenger, W., and Krauss, N. (2001) Three-dimensional structure of cyanobacterial photosystem I at 2.5 Å resolution, *Nature 411*, 909−917.
2. Fromme, P., Jordan, P., and Krauss, N. (2001) Structure of photosystem I, *Biochim. Biophys. Acta 1507*, 5−31.
3. Käss, H., Fromme, P., Witt, H. T., and Lubitz, W. (2001) Orientation and electronic structure of the primary donor radical cation $P700^{+\bullet}$ in photosystem I: A single crystals EPR and ENDOR study, *J. Phys. Chem. B 105*, 1225−1239.
4. Breton, J., Nabedryk, E., and Leibl, W. (1999) FTIR study of the primary electron donor of photosystem I (P700) revealing delocalization of the charge in $P700^+$ and localization of the triplet character in $^3P700$, *Biochemistry 38*, 11585−11592.
5. Wang, R., Sivakumar, V., Li, Y., Redding, K., and Hastings, G. (2003) Mutation induced modulation of hydrogen bonding to P700 studied using FTIR difference spectroscopy, *Biochemistry 42*, 9889−9897.
6. Webber, A. N., Su, H., Bingham, S. E., Kass, H., Krabben, L., Kuhn, M., Jordan, R., Schlodder, E., and Lubitz, W. (1996) Site-directed mutations affecting the spectroscopic characteristics and midpoint potential of the primary donor in photosystem I, *Biochemistry 35*, 12857−12863.
7. Redding, K., MacMillan, F., Leibl, W., Brettel, K., Hanley, J., Rutherford, A. W., Breton, J., and Rochaix, J. D. (1998) A systematic survey of conserved histidines in the core subunits of Photosystem I by site-directed mutagenesis reveals the likely axial ligands of P700, *EMBO J. 17*, 50−60.
8. Krabben, L., Schlodder, E., Jordan, R., Carbonera, D., Giacometti, G., Lee, H., Webber, A. N., and Lubitz, W. (2000) Influence of the axial ligands on the spectral properties of P700 of photosystem I: a study of site-directed mutants, *Biochemistry 39*, 13012−13025.
9. Hastings, G., Ramesh, V. M., Wang, R., Sivakumar, V., and Webber, A. (2001) Primary donor photo-oxidation in photosystem I: a re-evaluation of (P700(+) − P700) Fourier transform infrared difference spectra, *Biochemistry 40*, 12943−12949.
10. Prisner, T. F., McDermott, A. E., Un, S., Norris, J. R., Thurnauer, M. C., and Griffin, R. G. (1993) Measurement of the g-tensor of the $P700^{+\bullet}$ signal from deuterated cyanobacterial photosystem I particles, *Proc. Natl. Acad. Sci. U.S.A. 90*, 9485−9488.
11. Bratt, P. J., Rohrer, M., Krzystek, J., Evans, M. C. W., Brunel, L.-C., and Angerhofer, A. (1997) Submillimeter High-Field EPR Studies of the Primary Donor in Plant Photosystem I $P_{700}^{\bullet+}$, *J. Phys. Chem. B 101*, 9686−9689.
12. MacMillan, F., Rohrer, M., Krzystek, J., Brunel, L. C., and Rutherford, A. W. (1998) A high-field/high-frequency EPR characterization of the primary donor (P^+) in bacterial and plant photosynthetic reaction centers, *Photosynth.: Mech. Eff., Proc. Int. Congr. Photosynth., 11th 2*, 715−718.
13. Bratt, P. J., Poluektov, O. G., Thurnauer, M. C., Krzystek, J., Brunel, L.-C., Schrier, J., Hsiao, Y.-W., Zerner, M., and Angerhofer, A. (2000) The g-Factor Anisotropy of Plant Chlorophyll $a^{\bullet+}$, *J. Phys. Chem. B 104*, 6973−6977.
14. Burghaus, O., Rohrer, M., Götzinger, T., Plato, M., and Möbius, K. (1992) A novel high-field/frequency EPR and ENDOR spectrometer operating at 3 mm wavelength, *Meas. Sci. Technol. 3*, 765−774.
15. Feher, G. (1959) Electron spin resonance experiments on donor in silicon. I. Electronic structure of donors by the electron nuclear double resonance technique, *Phys. Rev. 114*, 1219−1244.
16. Webber, A. N., and Lubitz, W. (2001) P700: the primary electron donor of photosystem I, *Biochim. Biophys. Acta 1507*, 61−79.

17. Käss, H., and Lubitz, W. (1996) Evaluation of 2D-ESEEM Data of ^{15}N-Labeled Radical Cations of the Primary Donor P_{700} in Photosystem I and of Chlorophyll *a*, *Chem. Phys. Lett. 251*, 193−203.
18. Käss, H. (1995) Die Struktur des primären Donators P700 in Photosystem I: Untersuchungen mit Methoden der stationären und gepulsten Elektronspinresonanz, Thesis, Technische Universität, Berlin.
19. Käss, H., Bittersmann-Weidlich, E., Andréasson, L.-E., Bönigk, B., and Lubitz, W. (1995) ENDOR and ESEEM of ^{15}N labelled Radical Cations of Chlorophyll a and the Primary Donor P700 in Photosystem I, *Chem. Phys. 194*, 419−432.
20. Witt, H., Schlodder, E., Teutloff, C., Niklas, J., Bordignon, E., Carbonera, D., Kohler, S., Labahn, A., and Lubitz, W. (2002) Hydrogen bonding to P700: site-directed mutagenesis of threonine A739 of photosystem I in *Chlamydomonas reinhardtii*, *Biochemistry 41*, 8557−8569.
21. Li, Y., Lucas, M.-G., Konovalova, T., Abbott, B., MacMillan, F., Petrenko, A., Sivakumar, V., Wang, R., Hastings, G., Gu, F., van Tol, J., Brunel, L.-C., Timkovich, R., Rappaport, F., and Redding, K. (2004) Mutation of the putative hydrogen-bond donor to P700 of Photosystem I (submitted to *Biochemistry*).
22. Dorlet, P., Xiong, L., Sayre, R. T., and Un, S. (2001) High field EPR study of the pheophytin anion radical in wild type and D1-E130 mutants of photosystem II in *Chlamydomonas reinhardtii*, *J. Biol. Chem. 276*, 22313−22316.
23. Sundholm, D. (2000) Comparison of the electronic excitation spectra of chlorophyll a and pheophytin a calculated at density functional theory level, *Chem. Phys. Lett. 317*, 545−552.
24. Sundholm, D. (1999) Density functional theory calculations of the visible spectrum of chlorophyll a, *Chem. Phys. Lett. 302*, 480−484.
25. Jordan, R., Nessau, U., and Schlodder, E. (1998) Charge recombination between the reduced iron−sulfur clusters and $P700^+$, in *Photosynth.: Mech. Eff., Proc. Int. Congr. Photosynth., 11th*, 663−666.
26. Chirino, A. J., Lous, E. J., Huber, M., Allen, J. P., Schenck, C. C., Paddock, M. L., Feher, G., and Rees, D. C. (1994) Crystallographic analyses of site-directed mutants of the photosynthetic reaction center from *Rhodobacter sphaeroides*, *Biochemistry 33*, 4584−4593.
27. Zech, S. G., Hofbauer, W., Kamlowski, A., Fromme, P., Stehlik, D., Lubitz, W., and Bittl, R. (2000) A structural model for the charge separated state $P_{700}^{\bullet+}A_1^{\bullet-}$ in photosystem I from the orientation of the magnetic interaction tensors, *J. Phys. Chem. B 104*, 9728−9739.
28. Plato, M., and Moebius, K. (1995) Structural characterization of the primary donor in photosynthetic bacteria by its electronic g-tensor, *Chem. Phys. 197*, 289−295.
29. Huber, M., and Toerring, J. T. (1995) High-field EPR on the primary electron donor cation radical in single crystals of heterodimer mutant reaction centers of photosynthetic bacteria: first characterization of the G-tensor, *Chem. Phys. 194*, 379−385.
30. Hofmann, E., Wrench, P. M., Sharples, F. P., Hiller, R. G., Welte, W., and Diederichs, K. (1996) Structural basis of light harvesting by carotenoids: peridinin-chlorophyll-protein from *Amphidinium carterae*, *Science 272*, 1788−1791.
31. O'Malley, P. J., and Collins, S. J. (2001) The effect of axial Mg ligation on the geometry and spin density distribution of chlorophyll and bacteriochlorophyll cation free radical models: a density functional study, *J. Am. Chem. Soc. 123*, 11042−11046.
32. Balaban, T. S., Fromme, P., Holzwarth, A. R., Krauss, N., and Prokhorenko, V. I. (2002) Relevance of the diastereotopic ligation of magnesium atoms of chlorophylls in photosystem I, *Biochim. Biophys. Acta 1556*, 197−207.
33. Hsiao, Y.-W., and Zerner, M. C. (1999) Calculating ESR G tensors of doublet radicals by the semiempirical INDO/S method, *Int. J. Quantum Chem. 75*, 577−584.
34. Neese, F. (2001) Prediction of electron paramagnetic resonance *g* values using coupled perturbed Hartree−Fock and Kohn−Sham theory, *J. Chem. Phys. 115*, 11080−11096.
35. Kaupp, M., Remenyi, C., Vaara, J., Malkina, O. L., and Malkin, V. G. (2002) Density functional calculations of electronic g-tensors for semiquinone radical anions. The role of hydrogen bonding and substituent effects, *J. Am. Chem. Soc. 124*, 2709−2722.
36. Malkina, O. L., Vaara, J., Schimmelpfennig, B., Munzarova, M., Malkin, V. G., and Kaupp, M. (2000) Density Functional Calculations of Electronic g-Tensors Using Spin−Orbit Pseudopotentials and Mean-Field All-Electron Spin−Orbit Operators, *J. Am. Chem. Soc. 122*, 9206−9218.
37. Fuchs, M. R., Schnegg, A., Plato, M., Schulz, C., Muh, F., Lubitz, W., and Mobius, K. (2003) The primary donor cation $P^{+\bullet}$ in photosynthetic reaction centers of site-directed mutants of *Rhodobacter sphaeroides*: g-tensor shifts revealed by high-field EPR at 360 GHz/12.8 T, *Chem. Phys. 294*, 371−384.
38. Johnson, E. T., Mueh, F., Nabedryk, E., Williams, J. C., Allen, J. P., Lubitz, W., Breton, J., and Parson, W. W. (2002) Electronic and Vibronic Coupling of the Special Pair of Bacteriochlorophylls in Photosynthetic Reaction Centers from Wild-Type and Mutant Strains of *Rhodobacter sphaeroides*, *J. Phys. Chem. B 106*, 11859−11869.
39. Artz, K., Williams, J. C., Allen, J. P., Lendzian, F., Rautter, J., and Lubitz, W. (1997) Relationship between the oxidation potential and electron spin density of the primary electron donor in reaction centers from *Rhodobacter sphaeroides*, *Proc. Natl. Acad. Sci. U.S.A. 94*, 13582−13587.
40. Faller, P., Rutherford, A. W., and Un, S. (2000) High-Field EPR Study of Carotenoid$^{\bullet+}$ and the Angular Orientation of Chlorophyll$^{\bullet+}$ in Photosystem II, *J. Phys. Chem. B 104*, 10960−10963.
41. Lakshmi, K. V., Poluektov, O. G., Reifler, M. J., Wagner, A. M., Thurnauer, M. C., and Brudvig, G. W. (2003) Pulsed high-frequency EPR study on the location of carotenoid and chlorophyll cation radicals in photosystem II, *J. Am. Chem. Soc. 125*, 5005−5014.
42. Zouni, A., Witt, H. T., Kern, J., Fromme, P., Krauss, N., Saenger, W., and Orth, P. (2001) Crystal structure of photosystem II from *Synechococcus elongatus* at 3.8 Å resolution, *Nature 409*, 739−743.
43. Kamiya, N., and Shen, J. R. (2003) Crystal structure of oxygen-evolving photosystem II from *Thermosynechococcus vulcanus* at 3.7-Å resolution, *Proc. Natl. Acad. Sci. U.S.A. 100*, 98−103.
44. Poluektov, O. G., Utschig, L. M., Schlesselman, S. L., Lakshmi, K. V., Brudvig, G. W., Kothe, G., and Thurnauer, M. C. (2002) Electronic Structure of the P700 Special Pair from High-Frequency Electron Paramagnetic Resonance Spectroscopy, *J. Phys. Chem. B 106*, 8911−8916.

BI035466J